J Solid State Electrochem (2005) 9: 43–54
DOI 10.1007/s10008-004-0559-0

ORIGINAL PAPER

V. V. Panić · A. B. Dekanski · T. R. Vidaković
V. B. Mišković-Stanković · B. Ž. Javanović
B. Ž. Nikolić

Oxidation of phenol on RuO_2–TiO_2/Ti anodes

Received: 13 December 2003 / Accepted: 25 March 2004 / Published online: 3 July 2004

Abstract The oxidation of phenol on the RuO_2–TiO_2/Ti electrode has been studied by cyclic voltammetry, polarization measurements, electrochemical impedance spectroscopy and potentiostatic transients in H_2SO_4 and NaCl aqueous solutions. A reaction path with polymerization as the main reaction and side reactions after the initial step, similar to the reaction path on other electrode materials, is suggested. The formation of a phenoxy radical in a diffusion-controlled irreversible process is the initial step. The polymerization of phenoxy radicals leads to the formation of porous polyoxyphenylene film, strongly adherent to the electrode surface. The cyclic voltammetry measurements indicate side products, which could be, according to the literature, of quinone-like structure. Polyoxyphenylene film inhibits further oxidation of phenol, although complete electrode passivation was not observed. The presence of polyoxyphenylene film does not influence the pseudocapacitive behaviour of the electrode to a great extent, since the polyoxyphenylene film covers dominantly the coating surface, while active sites placed within coating cracks remain uncovered. The film seems to be permeable for hydrogen ions and water molecules.

Keywords Electrochemical impedance spectroscopy · Electrooxidation of phenol · Phenol polymerization · RuO_2–TiO_2/Ti electrode

V. V. Panić (✉) · A. B. Dekanski
Department of Electrochemistry, ICTM, Njegoševa 12,
P.O.B. 473, 11001 Belgrade, Serbia and Montenegro
E-mail: panic@tmf.bg.ac.yu
Tel.: +381-11-3232495
Fax: +381-11-3235255

T. R. Vidaković · V. B. Mišković-Stanković · B. Ž. Javanović
B. Ž. Nikolić
Faculty of Technology and Metallurgy,
University of Belgrade, Karnegijeva 4, P.O.B. 3503,
11120 Belgrade, Serbia and Montenegro

Introduction

Treatment of industrial wastewaters for removal of organic impurities, especially those containing phenol and chlorophenols, is a very important aspect of environmental technology. Electrooxidation of such impurities appears to be a promising process, since no additional oxidative reagents should be used [1], although electrochemical reactions, by which organic impurities from wastewater have to be oxidized, are connected with two common limitations. First, an appropriate anode material with good electrocatalytic activity for the oxidation of an appropriate organic compound has to be selected, and second, the oxidation reaction of impurities is, as a rule, subjected to mass-transport limitations, as a consequence of the low concentration of impurities.

The oxidation of phenol and substituted phenols has been investigated on a variety of metal anodes [2], with special attention being given to Pt [1, 2, 3, 4, 5, 6, 7, 8] and Au [6, 7], but also to Ag [9] and Ni–Nb–Pt–Sn alloy [10]. Owing to the good activity for total organic carbon removal, the anodes based on conductive metal oxides, such as PbO_2, SnO_2, IrO_2 and RuO_2 appear to be more promising materials for use in practical treatment of wastewaters containing organic impurities [8, 11, 12, 13, 14, 15, 16]. Recently, investigations of the activity of other nonmetal materials have been undertaken [1, 2, 17, 18, 19, 20]. Especially attractive are boron-doped diamond [17, 18], glassy carbon [19] and so-called quasi-3D materials, such as carbon felt [1, 2] and carbon black slurry electrodes [20], as highly-porous materials with large surface areas.

The first step in the electrooxidation of phenol and substituted phenols is the formation of phenoxy radicals [1, 6, 19, 20, 21], which can initiate the chain or branched polymerization, depending on the type of substitution in the phenol molecule [1, 3, 4, 19]. An alternative pathway of phenol electrooxidation is a combustion sequence that leads to the formation of quinone-like species, such

as hydroquinone and benzoquinone, followed by further oxidation to organic acids and finally to CO_2[6, 17, 20]. Complete mineralization can be achieved only at high current densities and low phenol concentration [17]. Low current densities and high phenol concentration are beneficial for polymerization, with aromatic compounds as the main products of side reactions [7, 17, 19]. The polymer formed strongly adheres to the electrode surface, making an insulating film that inhibits further phenol oxidation [3, 17, 19]. Musiani and coworkers [22, 23] investigated the properties of such a polymer electroformed on steel, and found that the film provides good protection against the corrosion of steel.

Dimensionally stable anodes (DSA), consisting of titanium-supported coatings of noble-metal oxides, seem to be very promising materials for this type of electrochemical reaction [11, 12, 13, 14, 15, 16], since they have large electrochemically active surface area, especially those prepared by the sol–gel procedure [25, 26], and high electrocatalytic activity for a number of electrochemical oxidation as well. Comninellis and coworkers [14, 15, 16] investigated the combustion of organics with simultaneous oxygen evolution from water on several DSA-type anodes and found that it occurs at oxide active sites where OH radicals are accumulated.

There is a lack of papers dealing with the phenol oxidation on DSA in the potential range of water stability. The aim of this work is to investigate the electrocatalytic activity of a RuO_2–TiO_2/Ti electrode prepared by the sol–gel procedure in the electrochemical oxidation of phenol and the changes in electrode properties during the oxidation. The oxidation was carried out at potentials lower than the potentials of the oxygen and/or chlorine evolution reaction. The effect of the polyoxyphenylene film formed on the electrochemical properties of the RuO_2–TiO_2 coating was also investigated.

Experimental

Electrode preparation

The oxide sols, used in the sol–gel procedure for titanium-supported RuO_2–TiO_2coating formation, were prepared by forced hydrolysis of $RuCl_3$ and $TiCl_3$ in extremely acid solutions (about 5.0 mol dm^{-3} HCl) as described elsewhere [24]. The chloride precursors were added in quantities that give about 1 mass % of a solid phase in the dispersion. The medium for RuO_2 sol preparation was aged for 46 h, while that for TiO_2 sol preparation was aged for 15 h. The oxide sols were then mixed in amounts that give the RuO_2(40 atom %)–TiO_2(60 atom %) coating composition. The parameters in the sol preparation procedure (acid medium composition and duration of forced hydrolysis) were adjusted for the preparation of the RuO_2(40 atom %)–TiO_2(60 atom %) coating, which is the coating with best activity and stability [25, 26]. The oxide coating was deposited onto a previously prepared titanium disk (7.2 mm in diameter) by multilayer application of an oxide sol mixture [25], which gave a total oxide amount on the electrode of 1.5 mg cm^{-2}. For each layer, the dispersing phase of the sol mixture was evaporated at 70 °C, and gel phase was afterwards calcined at 450 °C for 15 min. The final calcinations were performed at the same temperature for 30 min.

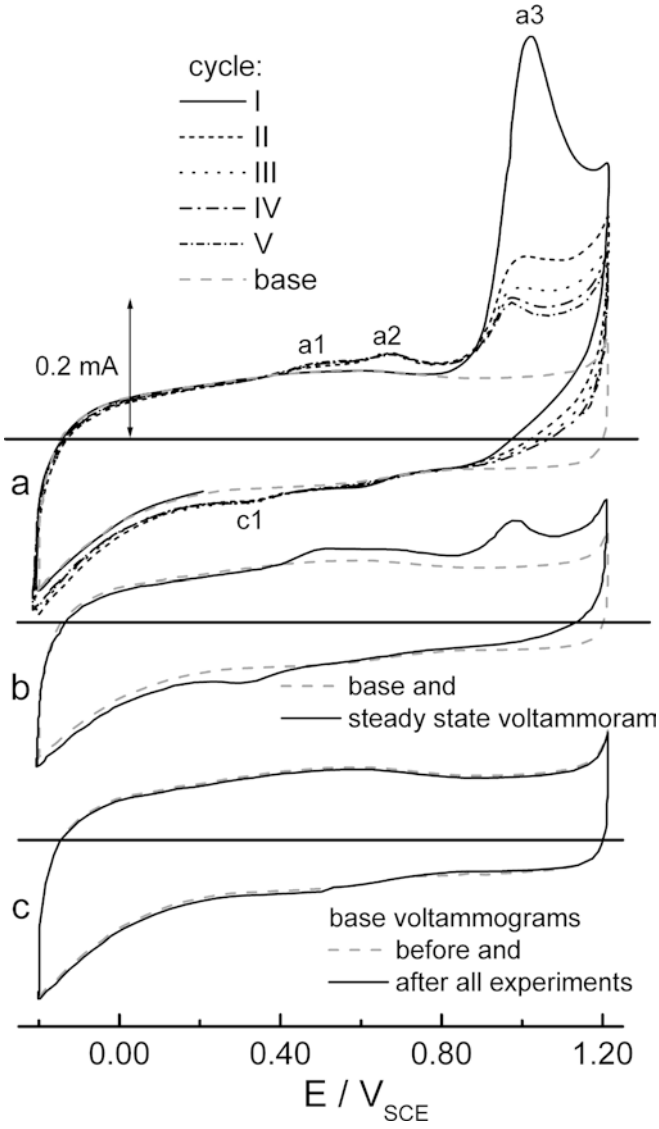

Fig. 1 *a* Cyclic voltammograms of a RuO_2(40 atom %)–TiO_2 (60 atom %)/Ti electrode recorded in 0.01 mol dm^{-3} C_6H_5OH + 0.5 mol dm^{-3} H_2SO_4water solution at room temperature; *b* base voltammogram, recorded in 0.5 mol dm^{-3} H_2SO_4, and steady-state voltammogram referred to 60 min of cycling in C_6H_5OH containing solution; *c* base voltammograms recorded before and after all experiments with phenol-containing solution. Sweep rate 20 mV s^{-1}

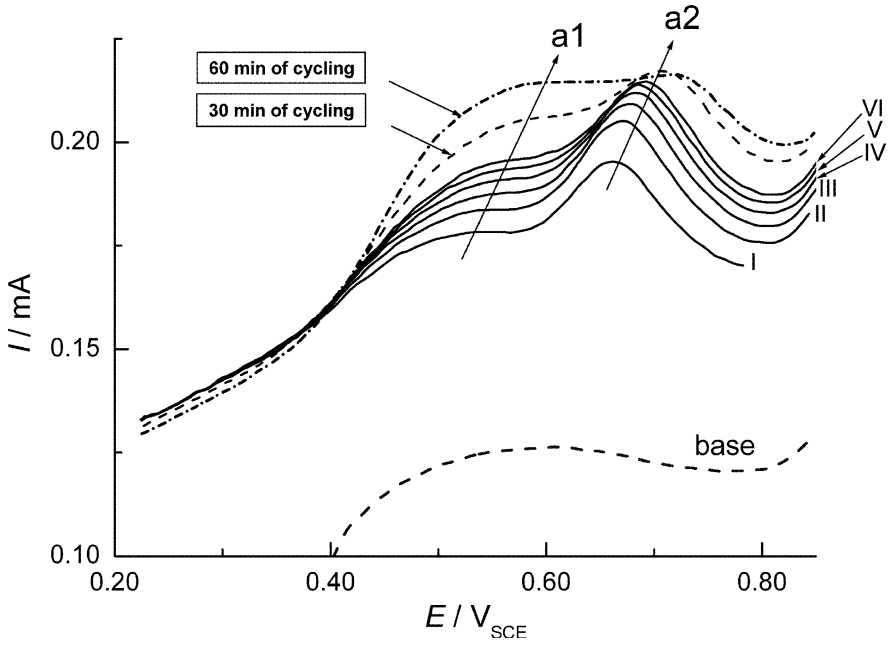

Fig. 2 Anodic part of the cyclic voltammograms from Fig 1, panel a shown within the potential window in which peaks *a1*and *a2* appear. The anodic part of the initial scan prior to phenol oxidation is marked as *base*

Solutions

Water (18 MΩ cm^{-1}) solutions of 0.5 mol $dm^{-3}H_2SO_4$ or 1.0 mol dm^{-3} NaCl, pH 2, were used as supporting electrolytes. The phenol solution was prepared from p.a. grade phenol (Chemapol, Czech Republic). An appropriate amount of phenol was dissolved in the supporting electrolyte to give a concentration of 0.01 mol dm^{-3}.

The cell

A one-compartment cell was used for electrochemical measurements. A Pt wire or a Pt gauze electrode was used as the counter electrode, while the saturated calomel electrode (SCE) served as the reference electrode. All experiments were carried out at room temperature.

Apparatus

The cyclic voltammetry, the polarization measurements and the potentiostatic transients were carried out with a PINE RDE4 potentiostat/galvanostat and with a CV-27 voltammograph (Bioanalytical Systems, USA). The electrochemical impedance spectroscopy (EIS) measurements on the electrode covered with polyoxyphenylene film were done in NaCl supporting electrolyte using 5 mV amplitude of sinusoidal voltage around the potential of 0.5 V_{SCE} over a frequency range from 100 kHz to 50 mHz. A PAR 5301 lock-in amplifier connected to a PAR 273A potentiostat/galvanostat was used. The impedance data were analysed using a suitable fitting procedure [27].

Results and discussion

The successive cyclic voltammograms of the RuO_2–TiO_2/Ti electrode, recorded in 0.01 mol $dm^{-3}C_6H_5OH$ and 0.5 mol $dm^{-3}H_2SO_4$ at 20 mV s^{-1} within the potential range of water stability, including the base voltammogram in supporting electrolyte are shown in Fig. 1, panel a. The voltammogram registered after 60 min of cycling, which could be assumed as the steady state, is shown in Fig. 1, panel b along with the base voltammogram. The base voltammograms in supporting electrolyte before and after all measurements with phenol containing electrolyte are shown in Fig. 1, panel c. The same voltammetric behaviour was recorded in NaCl supporting and NaCl–phenol electrolyte.

In the first scan, a very pronounced peak, a3, appears at a potential around 1.0 V_{SCE}, without the cathodic counterpart. In subsequent cycling, pair of peaks, a1–c1, and an anodic peak, a2, at around 0.5 and 0.7 V_{SCE}, respectively, are seen. In the course of cycling, the intensity of peak a3 decreases, while its position shifts towards the more negative potentials. Also, the pair a1–c1 and peak a2 fully develop. The development of peaks a1 and a2 is more clearly seen in Fig. 2. It is seen that the intensity of peak a1 increases with cycling, while the intensity of peak a2 reaches a constant value after about 30 min of cycling at 20 mV s^{-1}. The position of both peaks shifts towards the more positive potentials. The changes in intensity of cathodic peak c1 (not shown) are equivalent, although the changes in the peak position were not seen.

Peak a3 could be attributed to the formation of a phenoxy radical, which is the first step in phenol electrooxidation [1, 6, 7, 19]:

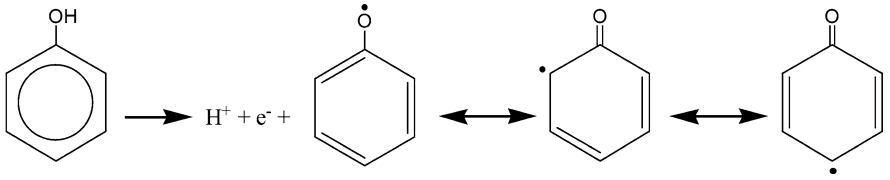

(1)

The polymerization of phenoxy radicals is the second reaction step. The inhibition of reaction 1, seen through the decrease in the intensity of peak a3 with cycling, is due to the continuous covering of the surface-active sites of oxide coating by the polyoxyphenylene film formed by radical polymerization [1, 3, 4, 7, 19].

In the investigation of phenol oxidation on Pt, Al-Maznai and Conway [1] obtained similar results concerning the cyclic voltammetry of the quinone/hydroquinone system. They registered kinetically irreversible behaviour of the quinone/hydroquinone system with a broad region of oxidation currents at potentials between 0.75 and 1.0 $V_{Pd/H}$, and one pronounced reduction peak at around 0.55 $V_{Pd/H}$. These observations are in line with the explanation of peaks a1/c1 and a2 in Figs. 1 and 2 as the formation and reaction of quinone-like species. Actually, the phenoxy radical formed in reaction (1) can be oxidized to the phenoxonium cation [28]:

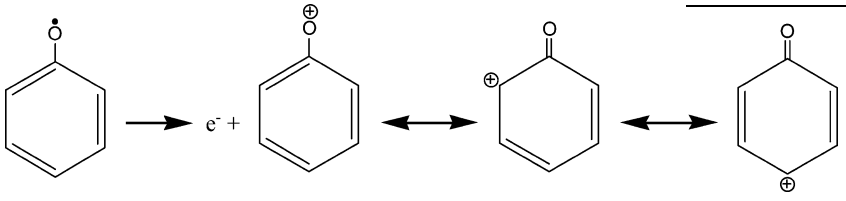

(2)

which in turn can undergo nucleophilic attack by water to form hydroquinone, i.e. the quinone/hydroquinone redox system should be expected:

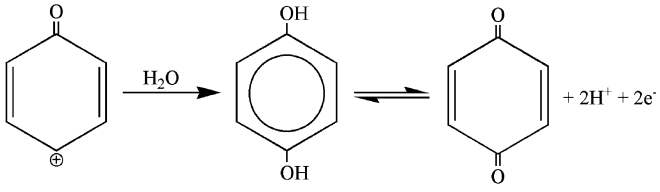

(3)

The difference in the shape of the base and the steady-state voltammograms in Fig. 1, panel b is seen in the potential regions of phenoxy radical formation and quinone/hydroquinone reaction. Outside these regions the two voltammograms overlap. This leads to the assumption that the polyoxyphenylene film on the electrode surface does not affect the electrode capacitive behaviour. The capacitive behaviour of the RuO_2-based electrode is caused by at least three separate contributions [29]. The most dominant is the pseudo-capacitive contribution from the solid-state surface redox transition that involves proton injection/ejection [30, 31]:

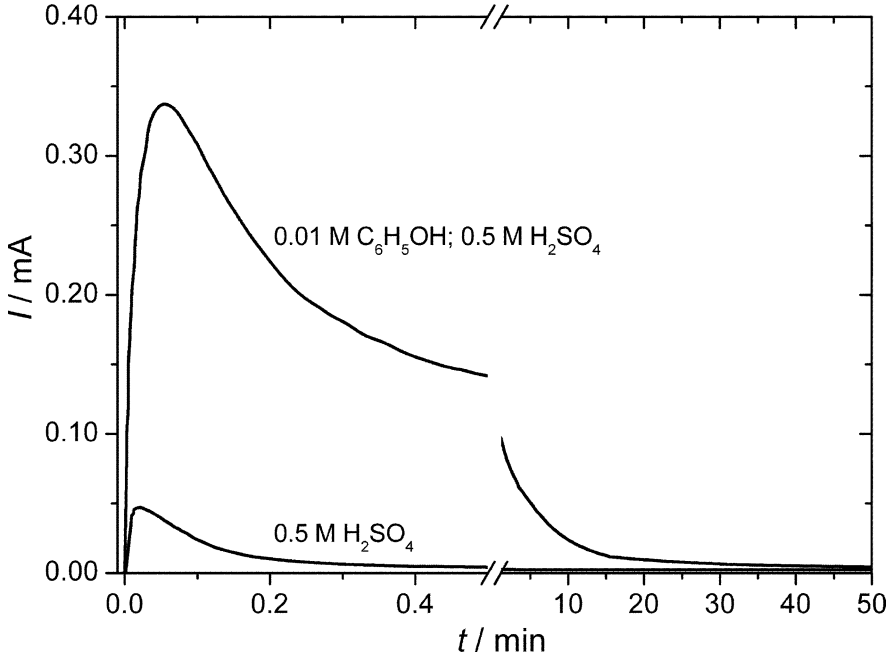

Fig. 3 Potentiostatic transients obtained for a RuO_2(40 atom %)–TiO_2(60 atom %)/Ti electrode in 0.5 mol dm^{-3} H_2SO_4 and in 0.01 mol dm^{-3} C_6H_5OH + 0.5 mol dm^{-3} H_2SO_4 at 1.0 V_{SCE}. Initial potential, prior to pulse, 0.80 V_{SCE}

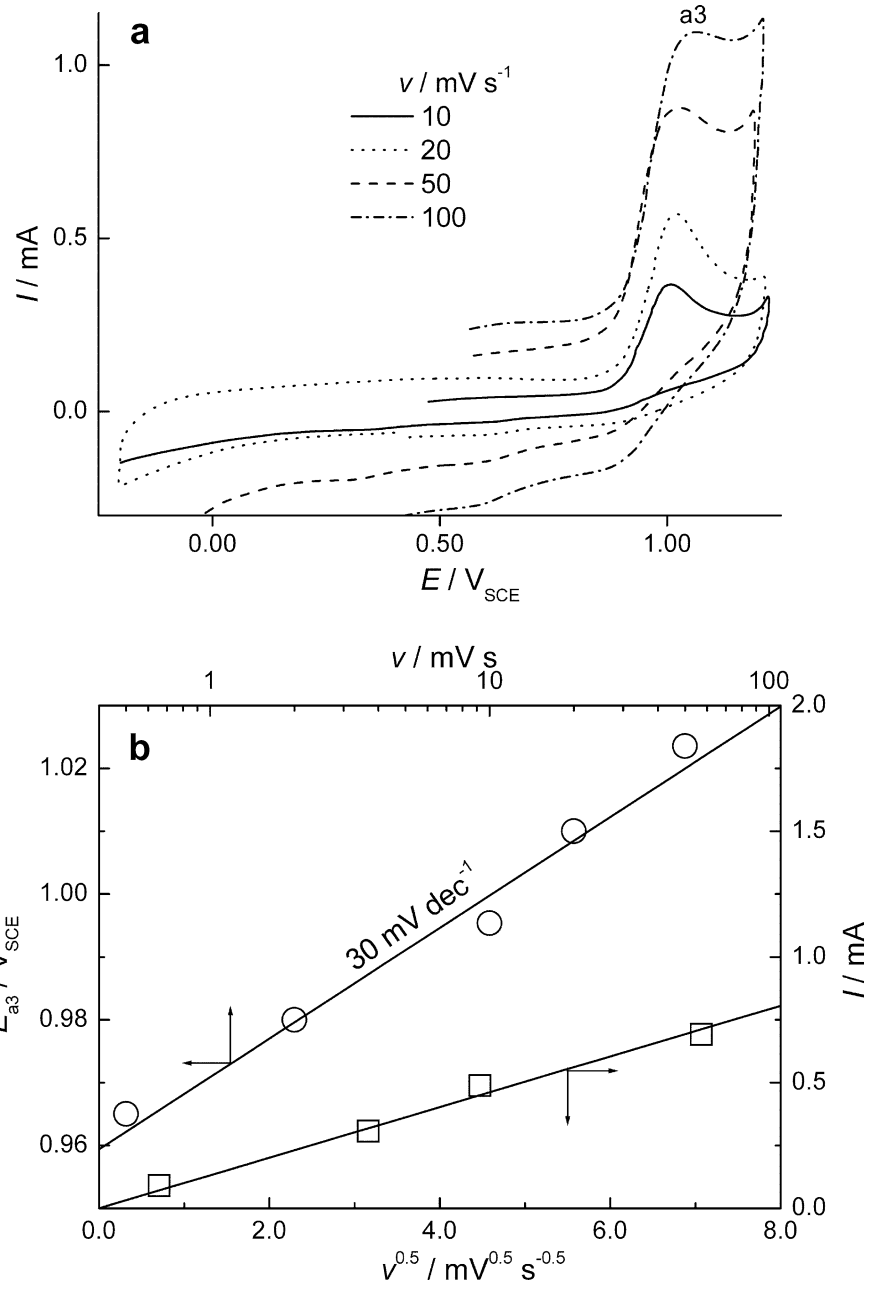

Fig. 4 a Initial cyclic voltammograms of a RuO_2(40 atom %)–TiO_2(60 atom %)/Ti electrode in 0.01 mol dm^{-3} C_6H_5OH + 0.5 mol dm^{-3} H_2SO_4at different scan rates and **b** the dependences of the peak a3 potential and current on scan rate

$$RuO_x + \delta H^+ + \delta e^- \rightleftharpoons RuO_{x-\delta}(OH)_\delta,\ 0 \leqslant \delta \leqslant x. \quad (4)$$

The polyoxyphenylene film formed in electrooxidation of phenol remains adsorbed on the surface after the removal of the electrode from a phenol-containing electrolyte [4, 23], so the coincidence of the voltammograms in Fig. 1, panel c confirms the assumption made from the similarity of the voltammograms in Fig. 1, panel b. Since the electrode pseudocapacitive behaviour is not disturbed, it can be concluded that the polyoxyphenylene film produced is permeable for the protons involved in reaction (4).

However, from the standpoint of the phenol oxidation reaction an additional comment can be made. Despite the decrease in the peak a3 current during the cycling, the peak still exists in the steady-state and complete inhibition of reaction (1) is not registered. This observation suggests that some of the active sites remain uncovered during the polymerization and maintain the activity for phenol oxidation.

The potentiostatic transients recorded at 1.0 V_{SCE} (near the potential of peak a3) in supporting electrolyte and in the presence of 0.01 mol dm^{-3} C_6H_5OH are shown in Fig. 3. Prior to the potential pulse, the electrode was kept at 0.80 V_{SCE} for 15 min.

The charging process in a supporting electrolyte is considerably faster than in the phenol-containing electrolyte. The current in the phenol-containing electrolyte

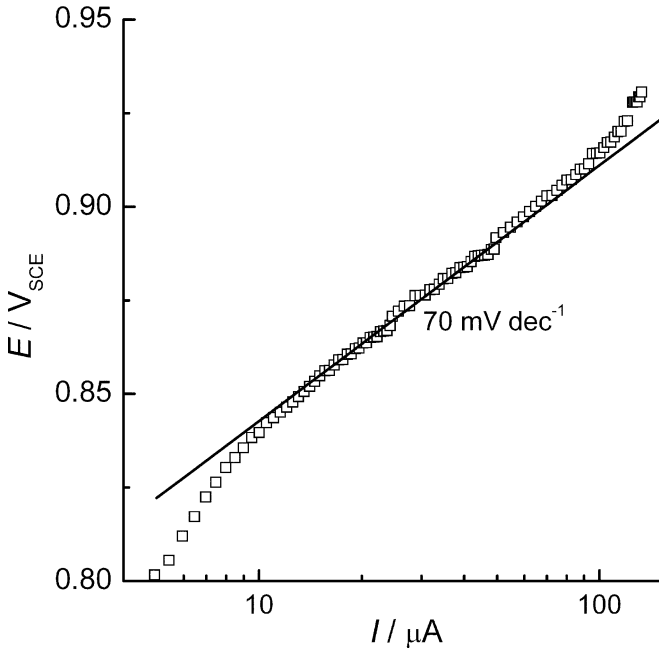

Fig. 5 Tafel plot for phenol oxidation on a RuO_2(40 atom %)–TiO_2(60 atom%)/Ti electrode in 0.01 mol dm^{-3} C_6H_5OH + 0.5 - mol dm^{-3} H_2SO_4; room temperature

is larger by approximately 1 order of magnitude and the decay is longer. As a consequence of increasing electrode coverage by the polyoxyphenylene film during the transient, the current asymptotically reaches the current plateau registered for the supporting electrolyte in approximately 50 min. This means that almost complete coverage of active sites is achieved during the potentiostatic transient, which is not the case in potential cycling up to the steady state (60 min). From this, one can conclude that the anode is covered with a greater amount of polyoxyphenylene film in the case of potentiostatic phenol oxidation than in potential cycling.

Taking into account the distribution of the active sites within the coating structure [25] and the theory of porous electrodes [32], the observed behaviour of the sol–gel-prepared RuO_2–TiO_2 coating in phenol oxidation can be commented on as follows. The anode electrochemically active surface can be considered as the outer and the inner active surface related to outer and inner active sites. While the former directly "faces" the electrolyte, the later is "hidden" within coating pores and cracks [25, 31]. In the early stages of phenol oxidation (first few cycles), reaction (1) is dominantly followed by polymerization at surface active sites owing to the relatively high phenol concentration. In the solution of low phenol concentration, parallel side reactions (2) and (3), with quinone structures as the products, are favoured [7, 17, 19]. Since the phenol concentration in coating pores and cracks is considerably lower than in the bulk of the electrolyte owing to mass-transfer limitations, these side reactions are dominant at inner active sites. As the oxidation proceeds, the surface-active sites are progressively covered by the polymer formed, while the reactions in the porous structure are not suppressed. In the steady state, reaction (1) occurs at the uncovered inner active sites, and phenoxy radicals undergo side reactions rather than polymerization. In the potentiostatic phenol oxidation the higher number of active sites in the bulk of the coating is accessible to the reacting species than in cyclic voltammetry conditions [31], where the diffusion of reacting species towards the inner active sites is slow compared with the sweep rate. This causes the polymerization reaction pathway to prevail also at the active sites placed deeper into the bulk of the coating in potentiostatic oxidation. Thus, the potentiostatically formed polymer film completely inhibits the oxidation, and the current reaches a value close to the value of the background current in the supporting electrolyte (Fig. 3).

The voltammetric curves are qualitatively the same at any applied scan rate. The first scans for different scan rates are shown in Fig. 4a. The intensity of peak a3 increases with scan rate, while the peak potential shifts towards positive values.

Figure 4b shows that the potential of peak a3 depends exponentially on the scan rate, while the peak currents, corrected for background current, show a linear dependence on the square root of the scan rate, which indicates a diffusion-controlled reaction. The slope of the E_{a3}–log $v$plot is close to 30 mV, which corresponds to the Tafel slope of 60 mV.

The Tafel plot for phenol oxidation, obtained from the first anodic linear sweep voltammogram at 0.5 mV s^{-1}, is given in Fig. 5. The plot shows a slope of about 70 mV, which is in fair agreement with the E_{a3}–log $v$data from Fig. 4b. Ureta-Zañartu et al. [19] also registered similar slope values for phenol oxidation on a glassy carbon electrode. This slope indicates that phenoxy radical formation could involve adsorption effects and/or subsequent chemical reaction. Iotov and Kalcheva [6] proposed the mechanism for phenoxy radical formation at Pt, Au and Pt/Au electrodes, in which the phenoxy radical formed remains adsorbed at the electrode surface and the polyoxyphenylene film is formed in the polymerization reaction of adsorbed radicals.

The influence of the electrode coverage with the polyoxyphenylene film produced on the Tafel slope and on the current of phenol oxidation is shown in Fig. 6. The plots for the upper potential limit of 1.10 V_{SCE} (prior to the oxygen evolution reaction) or 1.35 V_{SCE} (region of oxygen evolution) are shown in Fig. 6a. As can be seen, the change in the upper limit does not influence the electrode behaviour in phenol oxidation during successive anodic sweeps. The sharp decrease in current density between the first and the second run as well as the increase in the Tafel slope from 70 mV to about 110 mV are seen in Fig. 6b. The decrease in current density for two successive runs becomes less pronounced with cycling, while the slope increases by about 10 mV in each subsequent run, reaching a value of about 250 mV in the steady state.

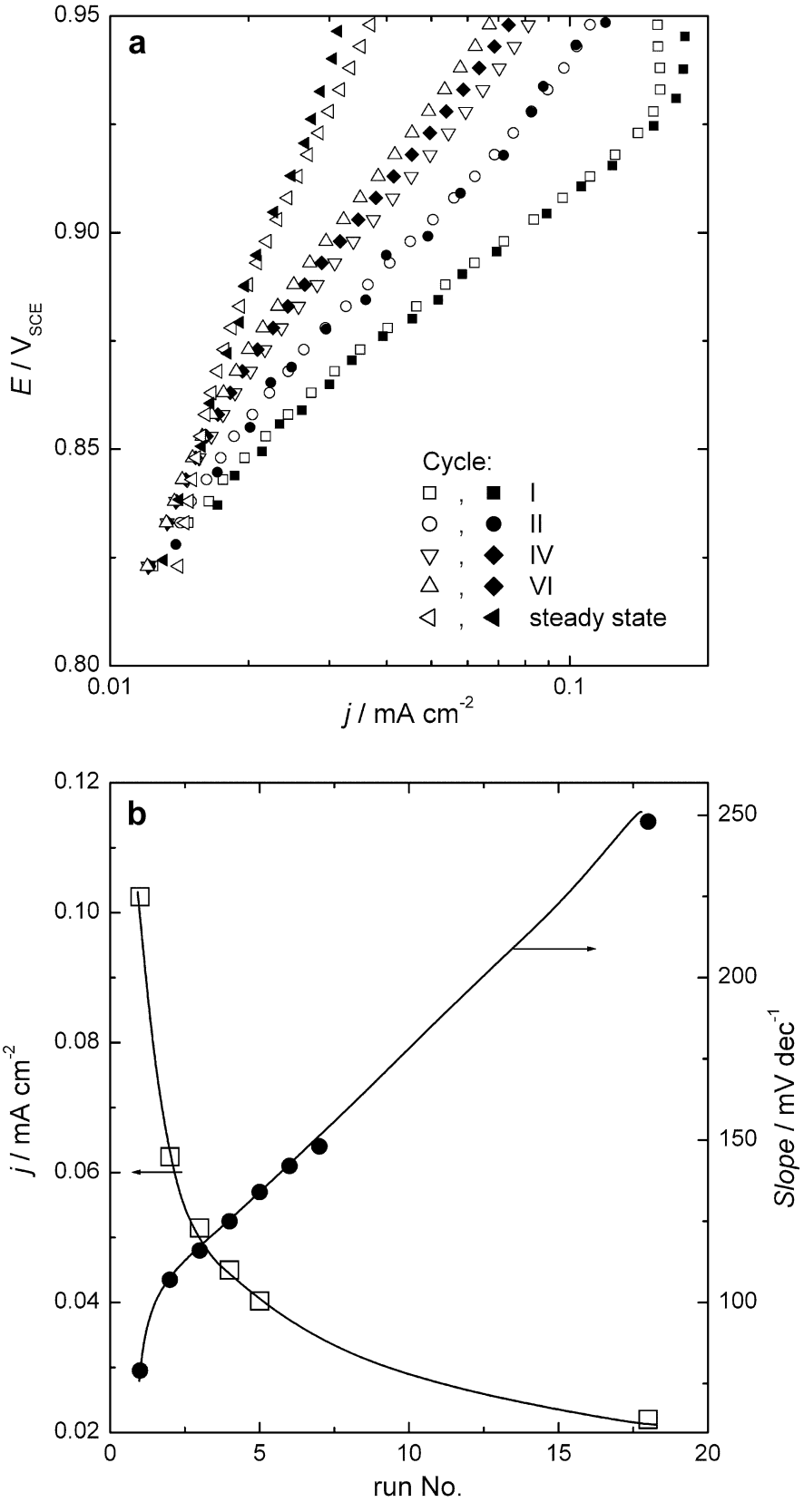

Fig. 6 a Tafel plots obtained by successive anodic sweeps of 0.5 mV s^{-1}(upper potential limits 1.1 V_{SCE}, *hollow symbols*, and 1.35 V_{SCE}, *full symbols*) on a RuO_2(40 atom %)–TiO_2(60 atom %)/Ti electrode in 0.01 mol dm^{-3} C_6H_5OH + 0.5 mol dm^{-3} H_2SO_4at room temperature and **b** the changes of the Tafel slope and the current density at 0.9 V_{SCE} as a function of the number of sweeps

The Tafel plots for the oxygen evolution reaction recorded in supporting H_2SO_4 electrolyte and in a phenol-containing electrolyte in the potential range from 1.10 to 1.35 V_{SCE} (immediately after phenol oxidation) are shown in Fig. 7. It can be concluded that the presence of the film does not influence con-

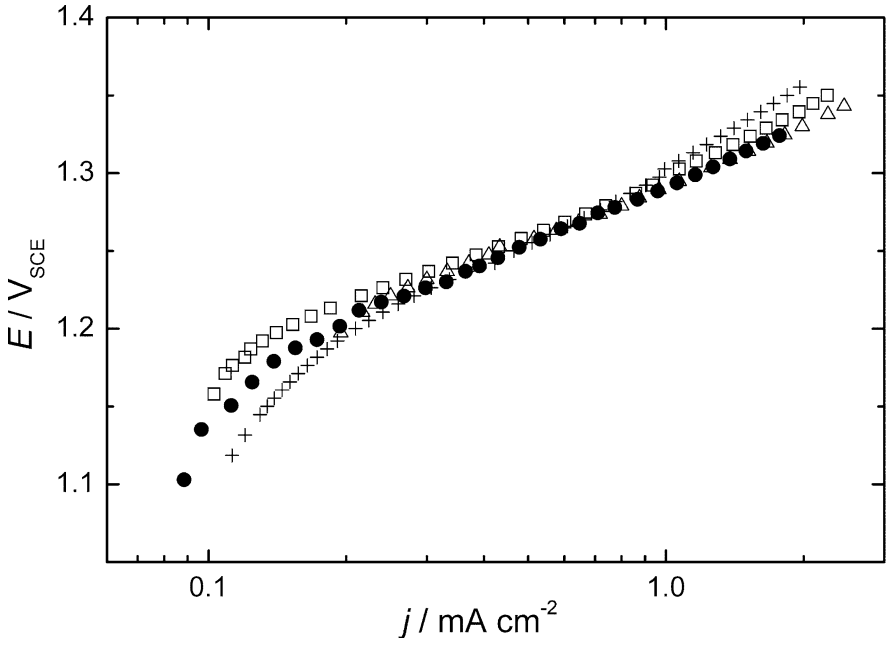

Fig. 7 Tafel plots for the oxygen evolution reaction on a RuO_2(40 atom %)–TiO_2(60 atom %)/Ti electrode recorded in 0.5 mol dm^{-3} H_2SO_4(*circles*), and in the presence of phenol in the first (*squares*), second (*triangles*) and steady-state (*crosses*) cycle; room temperature, sweep rate 0.5 mV s^{-1}

siderably the kinetics of the oxygen evolution reaction, which indicates the film permeability to the water molecules.

In order to obtain better insight into the properties of polyoxyphenylene film and into the influence of the film on the anode capacitive behaviour, EIS measurements were done. The impedance data for the electrode before phenol oxidation (state A, supporting electrolyte), after the steady state (state B) and after the potentiostatic phenol oxidation (state C) are shown in Fig. 8 as complex plane and Bode phase-angle plots. The data were recorded at a potential of 0.55 V_{SCE} (the capacitive region) in NaCl supporting electrolyte. The capacitive (i.e. pseudocapacitive) behaviour in all cases is registered in the low-frequency domain (curves A, B and C). The impedance behaviour of the electrode in state A is almost purely capacitive (Fig. 8a), while the behaviour of the electrode with different amounts of polyoxyphenylene film (curves B and C) indicates the capacitive response of the porous inner parts of the coating. This can be observed from the decreasing slope of the $-Z''$–Z' dependencies and decreasing phase angle of the Bode plots in the low-frequency domain going from curve A to curve C.

The influence of the polyoxyphenylene film is better seen from the impedance data collected in the high-frequency region. In this region, the almost vertical straight line for the electrode before phenol oxidation (Fig. 8a, curve A) transforms into the line with slope close to 45° for the electrodes covered by the film (curves B and C). Analysing the change from curve B to curve C, one can see that the frequency range, in which this straight line has a slope of 45°, extends to lower frequencies as the amount of polyoxyphenylene increases. This indicates slow diffusion of charged species involved in the electrode pseudocapacitive response through the polyoxyphenylene film-oxide coating system, as expected for the porous layers [27, 30]. These diffusion limitations become more pronounced as the amount of polymer increases.

The physical model of the electrode with the polyoxyphenylene film present on the surface can be discussed considering the equivalent electrical circuits (EEC) used to fit the experimental impedance data (Fig. 9). The circuits for the electrode related to curves A, B and C in Fig. 8 are represented in Fig. 9, while the simulation data are shown as solid lines along with the experimental data in Fig. 8b. The impedance data for the electrode without polymer film are fitted with simple EEC consisting of the electrolyte resistance, R_Ω, and a constant phase element related to the pseudocapacitive behaviour of the RuO_2–TiO_2 coating, Q, in series (Fig. 9a). The impedance of the constant phase element is given by the equation

$$\frac{1}{Z_{CPE}} = Y_0(j\omega)^n, \tag{5}$$

where Y_0, in $\Omega^{-1}s^n$ is the constant phase element constant, $j=(-1)^{1/2}$, ω, in units of radians per second, is the angular frequency and n is a dimensionless parameter that takes values between 0 and 1. For $n=1$ the constant phase element represents the capacitor, while for $n=0$ it becomes frequency-independent resistance. The constant phase element is often used in simulations to describe the double-layer capacitance of inhomogeneous surfaces and/or the quasi-3D surface of porous electrodes. In this case, n takes values between 0.5 (highly branched porous systems) and 1 (ideally flat surfaces).

In Fig. 9A, Q is related to the pseudocapacitive contribution of both outer and inner coating active sites. In order to fit the impedance data for the electrode after

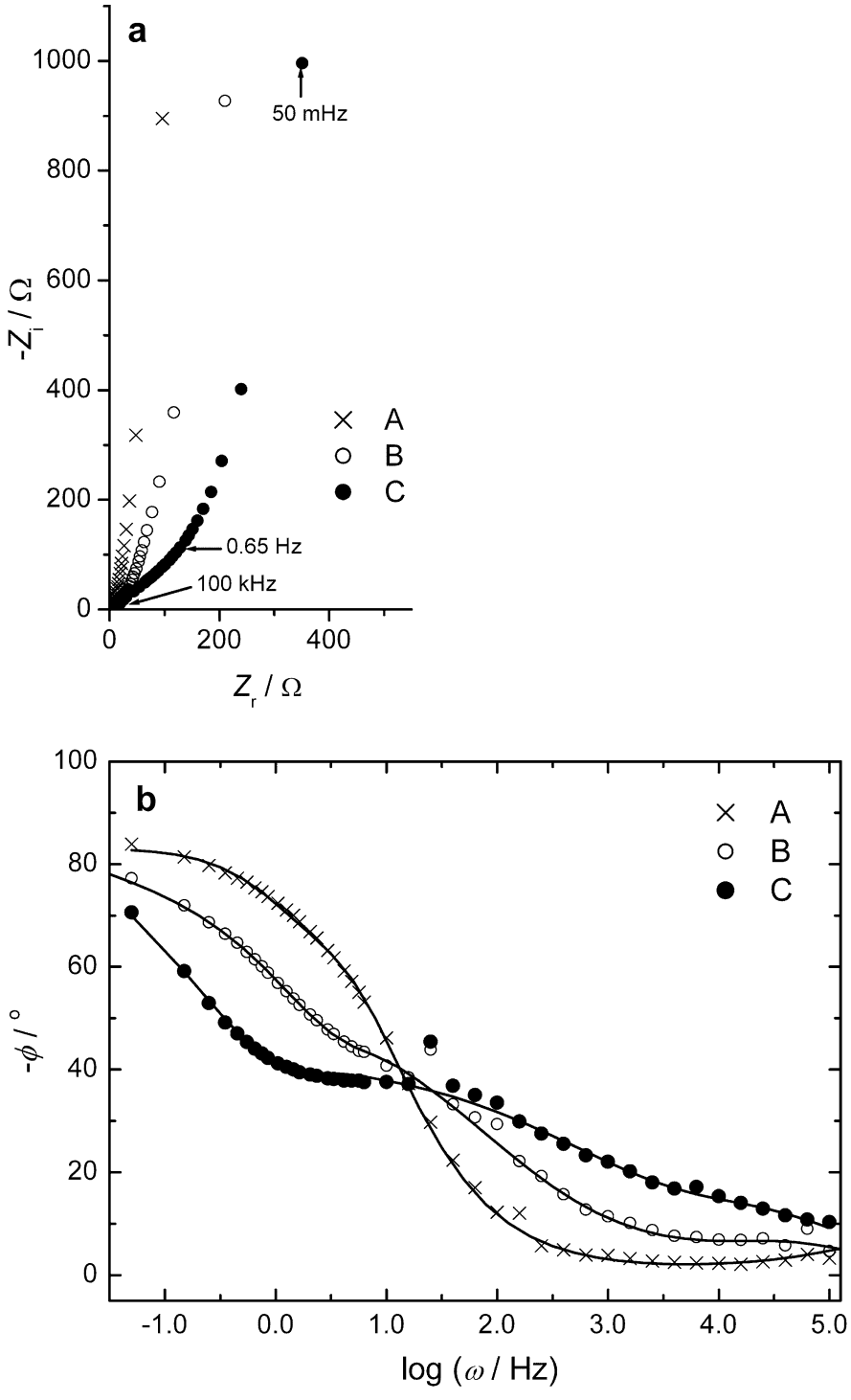

Fig. 8 a Impedance diagrams in the complex plane and **b** Bode phase-angle plots for a RuO_2(40 atom %)–TiO_2(60 atom %)/Ti electrode before phenol oxidation (*A*), after the steady state (*B*) and after potentiostatic oxidation (*C*)

phenol oxidation, two constant phase elements have to be included in the EEC. They indicate the separate response of outer (Q_{out}) and the inner (Q_{in}) active sites of the RuO_2–TiO_2 coating covered by polyoxyphenylene film (Fig. 9B, C), which were seen in state A as the mutual capacitive response. Additionally, these circuits include the pore resistance, R_p, and the porous Warburg element, *T*, which describes the diffusion through the porous layer of finite thickness [27]. The impedance of the *T* element is given by the equation

$$\frac{1}{Z_T} = \left(Y_0\sqrt{j\omega}\right)\tanh\left(B\sqrt{j\omega}\right), \tag{6}$$

where *B*, in units of seconds to the half power, is the time constant parameter. At high frequencies ($\omega > 2/B^2$) the *T* element behaves as the Warburg impedance, while at low frequencies it behaves as *R* and *C* in series, with $R = (B/Y_0)/3$.

In Fig. 9B and C the *T* element relates to the polyoxyphenylene film on the coating surface, while the *B*

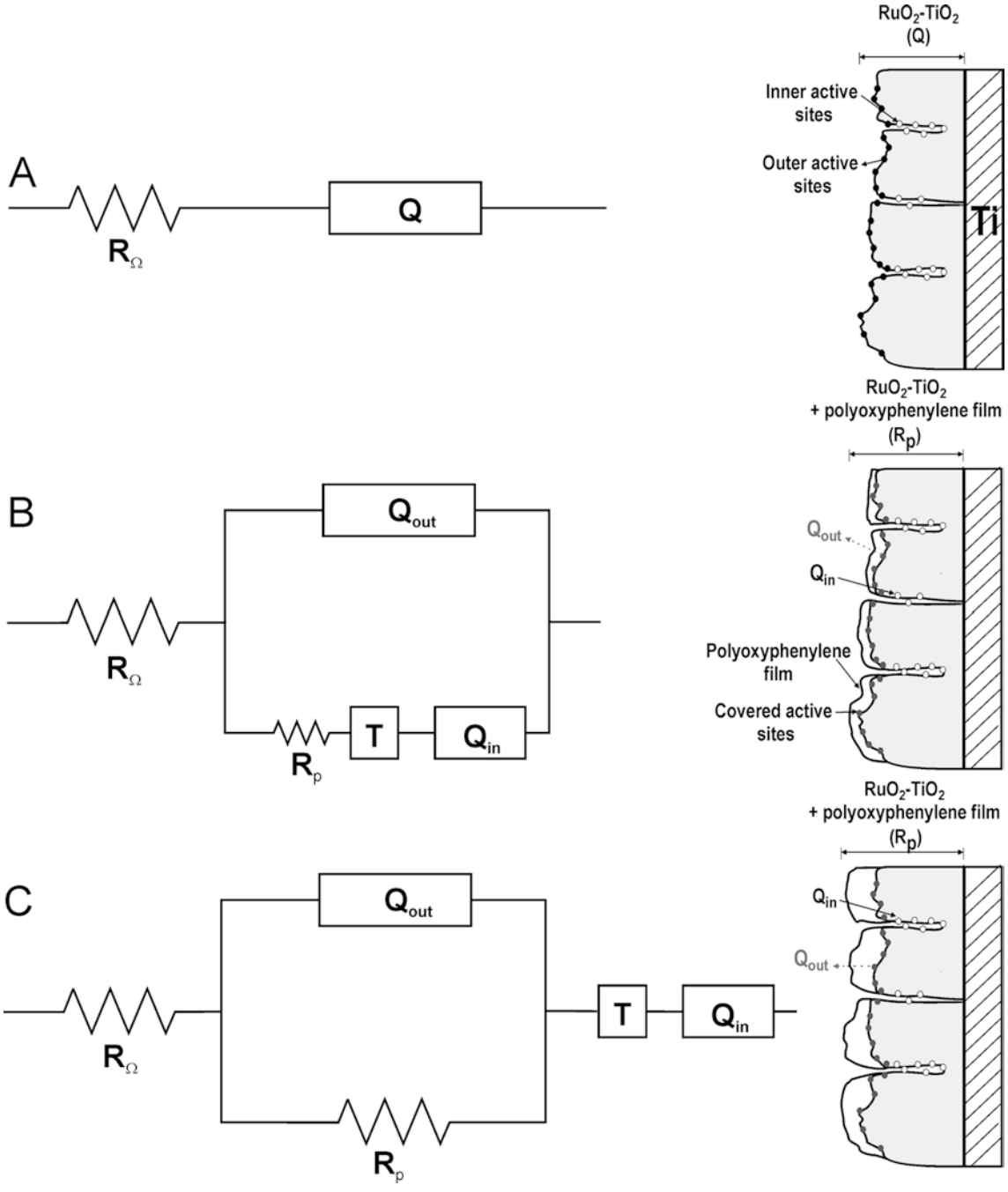

Fig. 9 Illustrations of a RuO_2–TiO_2/Ti electrode with a polyoxyphenylene film present on the surface and the equivalent electrical circuits used to fit the impedance data of the electrode **A** before phenol oxidation, **B** after the steady state and **C** after potentiostatic oxidation

parameter characterizes the time it takes for protons to diffuse through the film. The capacitive response of inner active sites is represented by a separate circuit branch (Fig. 9B), which is not included in the absence of the film on the coating surface (Fig. 9A).

The mean values of the parameters for the elements of the characteristic equivalent circuits are listed in Table 1. The relative deviation from the mean values was below 15% for all parameters. The Y_0 value of Q in state A is quite similar to the Y_0 values of Q_{in} (having in mind that Q_{out} is negligible in comparison with Q_{in}) for the electrode with the polymer film on the surface (states B and C), which is in accordance with cyclic voltammetry data (Fig. 1b, c) showing that the polymer film does not disturb the coating capacitive behaviour. Taking into account the transmission-line model for EEC of porous electrodes [30] and simple EEC from Fig. 9a, it can be assumed that Q in state A relates mainly to the capacitive response of the coating surface active sites. The Y_0 value of Q is higher than the Y_0

Table 1 The parameter values for the elements of equivalent electrical circuits shown in Fig. 9

Parameter		Electrode state		
		Before phenol oxidation	After steady-state voltammogram	After potentiostatic phenol oxidation
Q	Y_0/Ω^{-1} s^n	5.7×10^{-3}	–	–
	n	0.80	–	–
Q_{out}	Y_0/Ω^{-1} s^n	–	5.1×10^{-5}	1.0×10^{-4}
	n	–	0.75	0.72
Q_{in}	Y_0/Ω^{-1} s^n	–	5.5×10^{-3}	4.2×10^{-3}
	n	–	0.65	0.44
R_p/Ω		–	1.7	1.9
T	Y_0/Ω^{-1} s^n	–	1.1×10^{-3}	5.5×10^{-3}
	B/s$^{1/2}$	–	0.49	0.79

values of Q_{out} for states B and C, which indicates that not all of the coating outer active sites participate in Q_{out}, despite the permeability of the polymer film. The n values of Q_{out} are lower than the n value of Q owing to the difficult accessibility of electrolyte species to the outer active sites through the polymer film. As can be seen, the value of Y_0 of Q_{out} in state C is double the value obtained in state B. This can suggest that the polymer film formed potentiostatically is more permeable than that obtained during the cycling, despite the greater thickness of the former. The values of parameter n of Q_{in} in states B and C are quite close to 0.5, indicating slow diffusion of the electrolyte species that is included in the pseudocapacitive response of the inner part of the RuO_2–TiO_2 coating. The diffusion limitations become more pronounced with the increased amount of polymer (from state B to state C), which is indicated by the increasing values of the Y_0 and B parameters of the T element as well as by decreasing values of the parameters Y_0 and n of the Q_{in} element. This could be due to the decreasing diameter of pore orifices, which is also indicated by somewhat higher R_p value obtained in state C.

Conclusion

The first reaction step in the oxidation of phenol on a RuO_2(40 atom %)–TiO_2(60 atom %)/Ti electrode at the potentials prior to oxygen evolution is the formation of a phenoxy radical, which is irreversible, mass-transport controlled process involving an adsorption step. Polymerization of phenoxy radicals results in the formation of polyoxyphenylene film, strongly adherent to the electrode surface. The film hinders further phenol oxidation. The presence of side products of quinone-like structure, formed in the reactions parallel to the polymerization, is also seen.

The film appears to be permeable to protons and water molecules, so it does not disturb the pseudocapacitive properties of the electrode material or its electrocatalytic properties in oxygen evolution. The polyoxyphenylene film covers the surface-active sites, while those placed in the inner part of the RuO_2–TiO_2 coating remain uncovered. This is due to the lower phenol concentration within the coating pores, which favours the parallel reaction of quinone-like species formation. In the potentiostatic phenol oxidation, the inhibitive effect of the polymer film is more pronounced and persists in the inner coating region as well.

The impedance measurements confirm that the polyoxyphenylene film covers only the surface active sites of the RuO_2-TiO_2 coating, causing the pseudocapacitive response of the coating inner active sites to be diffusion-controlled. The diffusion limitations become more pronounced as the amount of polymer on the RuO_2–TiO_2 coating surface increases.

Acknowledgements The research was financially supported by the Ministry of Science, Technology and Development, Republic of Serbia, project no. 2-1230.

References

1. Al-Maznai H, Conway B (2001) J Serb Chem Soc 66:765
2. Bruno F, Pham MC, Dubois JE (1977) Electrochim Acta 22:451
3. Glarum SH, Marshall JH (1985) J Electrochem Soc 132:2939
4. Glarum SH, Mashall JH, Hellman MY, Taylor GN (1987) J Electrochem Soc 134:81
5. Lapuente R, Cases F, Garcés P, Marallón E, Vázquez JL (1998) J Electroanal Chem 451:163
6. Iotov PI, Kalcheva SV (1998) J Electroanal Chem 442:19
7. Ureta-Zañatu MS, Bustos P, Diez MC, Mora ML, Gutiérez C (2001) Electrochim Acta 46:2545
8. Jedral W, Merica SG, Bunce NJ (1999) Electrochem Comm 1:108
9. Conway B, Ayranci E, Al-Maznai H (2001) Electrochim Acta 47:705
10. Sistiaga M, Pierna AR, Marzo FF, Altube A, Lorenzo A (1998) Appl Surf Sci 133:124
11. Feng YJ, Li XY (2003) Water Res 37:2399
12. Iniesta J, Expósito E, González-García J, Montiel V, Aldaz A (2002) J Electrochem Soc 149:D57
13. Stucki S, Kötz R, Carcer B, Suter W (1991) J Appl Electrochem 21:99
14. Comninellis C, Nerini A (1995) J Appl Electrochem 25:23
15. Comninellis C (1994) Electrochim Acta 39:1857
16. Comninellis C, Pulgarin C (1993) J Appl Electrochem 23:108
17. Iniesta J, Michaud PA, Panizza M, Cerisola G, Aldaz A, Comninellis C (2001) Electrochim Acta 46:3573
18. Hagans PL, Natishan PM, Stoner BR, O'Grady WE (2001) J Electrochem Soc 148:E298
19. Ureta-Zañatu MS, Bustos P, Berríos C, Diez MC, Mora ML, Gutiérez C (2002) Electrochim Acta 47:2399
20. Boudenne JL, Cerclier O, Galéa J, Van der Vlist E (1996) Appl Catal A 143:185
21. Gattrell M, Kirk D (1992) J Electrochem Soc 139:2736
22. Musiani M, Pagura C, Mengoli G (1985) Electrochim Acta 30:501
23. Mengoli G, Musiani M (1987) J Electrochem Soc 134:643C
24. Panić V, Dekanski A, Milonjić S, Atanasoski R, Nikolić B (1999) Colloids Surf A 157:269
25. Panić V, Dekanski A, Milonjić S, Atanasoski R, Nikolić B (2000) Electrochim Acta 46:415
26. Panić V, Dekanski A, Wang G, Fedoroff M, Milonjić S, Nikolić B (2003) J Colloid Interface Sci 263:68

27. Boucamp B (1989) Equivalent circuit (EQUIVCRTPAS) user's manual. University of Twente, Enschede, The Netherlands
28. Thompson MJ, Zeegers PJ (1989) Tetrahedron 45:191
29. Sugimoto W, Kizaki T, Yokoshima K, Murakami Y, Takasu Y (2004) Electrochim Acta 49:313
30. Conway B (1999) Electrochemical supercapacitors—Scientific fundamentals and technological applications. Plenum, New York
31. Ardizzone S, Fregonara G, Trasatti S (1990) Electrochim Acta 35:263
32. Chizmadzev Y, Chirkov Y (1983) In: Yeager E, Bockris J, Conway B, Sarangapani S (eds) Comprehensive treatise of electrochemistry, vol 6. Plenum, New York, pp 317–393